Proceedings of the 2019 Hypervelocity Impact Symposium
HVIS2019
April 14-19, 2019, Destin, FL, USA
HVIS2019-051

Shear band characteristics in high strain rate naval applications

Michael J. P. Conway[a], James D. Hogan[a]*

[a]*Department of Mechanical Engineering, University of Alberta, Edmonton, AB T6G 2R3, Canada*

Abstract

This paper explores the dynamic behavior of HSLA 65 naval steels, specifically focusing on the initiation and growth of shear bands in quasi-static and dynamic compression experiments and how these bands affect stress-strain responses. The results indicate that the yield strength for this HSLA 65 increases from 541 ± 8 MPa for quasi-static (10^{-3} s^{-1}) to 1081 ± 48 MPa for dynamic rates 1853 ± 31 s^{-1}, and the hardening exponent increases from 0.376 ± 0.028 for quasi-static to 0.396 ± 0.006 for dynamic rates. Yield behavior was found to be associated with the onset of shear banding for both strain-rates, confirmed through visualization of the specimen surface using high-speed and ultra-high-speed cameras. For the quasi-static case, shear banding and yielding was observed to occur at 2.5% strain, and were observed to grow at speeds of upwards of 38 mm/s. For the dynamic experiments, the shear banding begins at approximately 1.18 ± 0.06% strain and these can grow upwards of 2122 ± 213 m/s during post-yield softening. Altogether, these measurements are some of the first of their kind in the open literature, and provide guidance on the critical time and length scales in shear banding. This information can be used in the future to design more failure-resistant steels, which has broader applications in construction, defense, and natural resource industries.

Keywords: shear band; dynamic failure; steel; split-hopkinson pressure bar; digital image correlation

Nomenclature

n	strain hardening coefficient
K	strength coefficient (MPa)
Greek symbols	
ε	strain (mm/mm)
σ	stress (MPa)
Subscripts	
f	flow stress (MPa)

1. Introduction

Shear bands are an important topic in understanding the mechanics of materials as it is a dominant failure mechanism and precursor for crack initiation and propagation at high strain rates in many materials [1]. For example, shear bands are commonly observed in manufacturing and operation in the ship building [2], rail transportation [3], and aerospace industries [4]. In these industries, the materials are exposed to a wide range of strain rates from quasi-static to explosive loading. With the ever-increasing expectations of steels being stronger and more cost effective, it becomes more important to develop a fundamental understanding of the failure of these materials. In these applications, the formation of shear bands plays a role in the failure and the stability of the material. Understanding these loading conditions and the behavior of shear bands (i.e. velocity, propagation direction and propensity) will improve the material selection process and the performance of newly developed materials for these industries.

* Corresponding author. Tel.: +1 780 492 7133.
E-mail address: jdhogan@ualberta.ca ; mjconway@ualberta.ca .

In the past, shear banding has been commonly observed in metals [1,5,6], polymers [7], and geologic [8] materials. Authors have studied shear banding through experiments [9,10], and through computational and analytical modelling [11,12]. Shear bands are commonly labelled as: 1. deformed shear bands, and 2. transformed shear bands, and these are mainly distinguished by whether a white etched hardened band is formed [13]. There has been several theories on the generation of shear bands in materials, including dynamic recrystallization (DRX) [14], grain deformation [13], rotational recrystallization [15], and phase transformation [16]. Regardless, shear bands are commonly believed to significantly affect material strength, stability, and have been noted to often be a precursor to cracking through the generation of voids [17]. Despite broad implications of shear banding to industry applications, the topic remains a very active area of research [1,12,18].

Motivated by these and many other past works, this paper focuses on studying the growth and evolution of shear bands in a high strength, low alloy steel, specifically HSLA 65. We study material behavior through mechanical testing in compressive stress-states and couple this testing to visualization of shear banding and failure using high-speed and ultra-high-speed cameras and Digital Image Correlation (DIC) techniques. Being able to pair visualization and quasi-static and dynamic loading events provides insight into the deformation of the material and, specifically, the propagation velocity, direction, and orientation of the shear bands on the surface of the specimen. The results are discussed in the context of our current understanding of shear banding in steels, especially discussing the strains at which they occur, the velocity they grow, and their effect on the stress-strain response.

2. Methodology

2.1. Material Tested

HSLA 65 (ASTM A945 [19]) was tested in compression, where specimens were removed from as-received steel plate that was 12” x 12” x 0.75” in size. This steel has been used on navy ships in Canada due to its cost effectiveness, weldability, and its high strength. The specimens were milled from the center of the thickness of the plate and were made in accordance with American Society for Testing and Materials (ASTM) standards following ASTM 09 for both specimen creation and testing. The HSLA 65 steel was specifically chosen due to the propagation of shear bands being clearly visible during the impact process. The chemical analysis of the HSLA 65 in this study is given in Table 1 and was provided from the manufacturer in the mill test certificate.

Table 1. Components of HSLA 65 (wt.% are listed)

C	Mn	P	S	Si	Cu	Ni	Cr	Mo	V	Ti	Al	B	Cb	N
0.08	1.43	0.020	0.004	0.299	0.020	0.01	0.04	0.006	0.067	0.016	0.030	0.0002	0.035	0.008

2.2. Quasi-static Testing

Compression tests were performed on a MTS 810 testing machine for rectangular specimens of size 5.00 mm x 4.00 mm x 3.50 mm using displacement control. The quasi-static tests were performed at a nominal strain rate of 10^{-3} s^{-1}. This specimen shape was selected for the ability to visualize the deformation on the surface of the specimen during experiments, as well as to perform Digital Image Correlation measurements. The displacement and force were recorded through the MTS machine at a sampling rate of 100 Hz, while the surface and deformation features of the specimen were recorded through the use of a PROMON one-megapixel camera with a macro lens recording at 100 frames per second, which matched the sampling frequency of the MTS machine. The strains were measured during testing using DIC techniques with the VIC2D commercial software. This approach consisted of applying a randomly distributed pattern over the surface of the specimen using an airbrush and trying to minimize the overall particle size through atomization given the small specimen size. This was achieved through the use of an ultra-fine point airbrush to apply black paint that resulted in a speckle diameter between 50 and 300 microns. The quality of the speckle pattern was checked in the VIC2D software to minimize error before experimentation. During testing, an ultra-bright LED light equipped with a 7.6 mm diameter liquid light guide was used to illuminate the specimen in a highly contrasted and overexposed condition. Once the data was obtained, the DIC data was paired with the captured load data from the universal testing machine and matched to the DIC strain data through physical events captured in both measurement techniques. In this case, a sharp unload was induced which was matched in time between the camera and MTS measurements. Using DIC, both small strains and large plastic strains can be resolved, whereas conventional strain gauges cannot be used to provide similar

measurements [20] without the need to apply compliance corrections for the universal testing machine. Additionally, a greater amount of data can be derived from the measurements given the ability to spatially resolve the strain across the surface of the specimen providing information such as local strains, displacement and ultimately verifying stress equilibrium.

2.3. Split-Hopkinson Pressure Bar Testing

A Split-Hopkinson Pressure Bar (SHPB) was used to perform dynamic compression measurements. The same specimen sizes were used in the dynamic experiments as the quasi-static experiments (5.00 mm x 4.00 mm x 3.50 mm), and the rectangular shapes were chosen for visualization purposes. The apparatus consisted of a 304.8 mm striker, 914.4 mm incident bar and a 1016 mm transmission bar that all have a diameter of 12.7 mm. The bars are made of Maraging C350 steel that has a minimum hardness of 52 HRC. The SHPB is an apparatus that takes an input from a striker that is fired from a gas gun. The striker then impacts a pulse shaper that is attached to the incident bar. This pulse shaper is used to shape the profile of the input pulse to achieve proper stress equilibrium and constant strain rate in the specimen [21]. In our experiments, mild steel with a diameter of 6.35 mm and a thickness of 0.635 mm was used, which follows from previous studies on improving stress equilibrium and reducing Pochhammer-Chree dispersion during SHPB testing [22,23]. The specimen and the pulse shaper are both placed with a small amount of high pressure grease to minimize friction between the interfaces [21]. Verification of stress equilibrium is performed through a force balance, which is found in reasonable agreement for all our tests. In these experiments, the surface of the specimen is recorded using a Kirana ultra-high-speed camera with a HBM GEN3i data acquisition system recording at 20 MHz. The data acquisition triggers the camera from the beginning rise of the incident pulse and the camera trigger pulse is recorded in the data set. The camera records 180 frames at 1 million frames per second with a resolution of 924 pixels x 768 pixels. At this frame rate and resolution, we can visualize deformation in materials at sufficient spatial and temporal resolution that are not widely reported in the literature.

3. Results

In this study we investigate the compressive behavior of HSLA 65 navy steel in quasi-static and dynamic loading conditions. To begin the analysis, we have shown three stress-strain curves for the quasi-static case and four stress-strain curves for dynamic case in Figure 1 to demonstrate the rate-effects and repeatability of the measurements. In quasi-static testing conditions at a strain rate of 0.001 s^{-1}, the yield strength of the HSLA 65 was found to be 541 ± 8 MPa, which are colored black in Figure 1. The yield stress found at a dynamic strain rate of 1853 ± 31 s^{-1} was 1081 ± 48 MPa (colored blue in Figure 1). These values are summarized in Table 2. The yield strengths and symmetrical limits are found from averaging the resulting values in each test and providing the standard deviation across the sample set. In quasi-static and dynamic loading of HSLA 65, there is a distinct yield point seen in the curves. For the quasi-static experiments, the yield strain is 0.93 ± 0.12 % and for the dynamic experiments, the yield strain is 1.05 ± 0.03 %. At the higher strain rates, this yield point is much more prominent, while the Pochhammer-Chree dispersion should be considered after the yielding of the material. Later, these yield features are linked to shear banding and failure in the material.

To further probe material behavior and generalize the results, the flow stress for this material was calculated using the true stress-true strain data for Equation (1).

$$\sigma_f = K\varepsilon^n \tag{1}$$

where the flow stress, σ_f, is the stress required to continue the plastic deformation of a metal. From Equation (1), K is the strength coefficient, ε is the plastic strain, and n is the hardening coefficient. Using a linear fit of the true strain-true stress data on a log-log scale, the strength coefficient for the quasi-static case is K = 2029 ± 172 MPa with a strain hardening coefficient of n = 0.376 ± 0.028. For the dynamic experiments, the strength coefficient is found to be K = 3098 ± 52 MPa and the hardening coefficient is n = 0.396 ± 0.006. These values are also summarized in Table 2 for both strain rates, along with the yield strength.

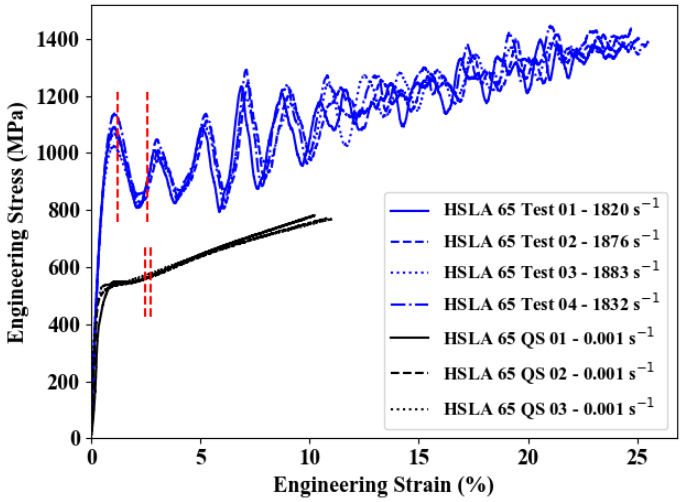

Figure 1. Engineering stress-strain curves of the tested HSLA 65 in quasi-static (black) and dynamic (blue) compression. The vertical lines indicate the region that shear band measurements were taken, which are linked with subsequent figures.

Table 2. Flow stress coefficients for HSLA 65 in quasi-static and dynamic compression.

Strain Rate (s^{-1})	Yield Strength (MPa)	K (MPa)	n
0.001	541 ± 8	2029 ± 172	0.376 ± 0.028
1853 ± 31	1081 ± 48	3098 ± 52	0.396 ± 0.006

Next, we investigate a series of high-speed camera images for the quasi-static experiments, which are shown in Figure 2, and dynamic experiments that are shown in Figure 3. In Figure 2, the collection of images were chosen that represents notable stages in shear band development in the quasi-static experiment: Figure 2a shows the intact surface before localizations occur; Figure2b shows localizations forming on the surface at 45° to the loading direction with the predominant bands developing from the edges and propagating inwards until they meet; Figure 2c shows the surface at which point the bands visually look consumed by the surface texturing that begins to develop at later stages of plastic deformation. The localizations began forming on the surface at approximately 2.5% strain. Next, shown in Figure 3 are a collection of high-speed camera images taken during a dynamic experiment that demonstrate the initiation and growth of shear banding. Figure 3a shows the specimen in pristine conditions. Figure 3b shows the surface at ~1% strain with the initial bands propagating across the surface. The initiation of the localizations occurs at the corners of the specimen and again propagate at approximately 45° angles. Across all the dynamic experiments, the initiation of these localizations on the surface begin at approximately 1.19 ± 0.06% strain. In comparison with the stress-strain curve (Figure 1), the localizations approximately begin around the yield of the material. Further, Figure 3c shows the specimen surface at ~2% strain, and this is when the bands begin to coalesce on the surface that is shown. The bands are the most visually distinct at this strain. At later strains (Figure 3d), we observe surface texturing occurring that consumes the shear bands on the surface and this continues until only the large and visually distinct localizations can be seen, which remain after the experiment. This occurs similarly to the quasi-static experiments (Figure 2c).

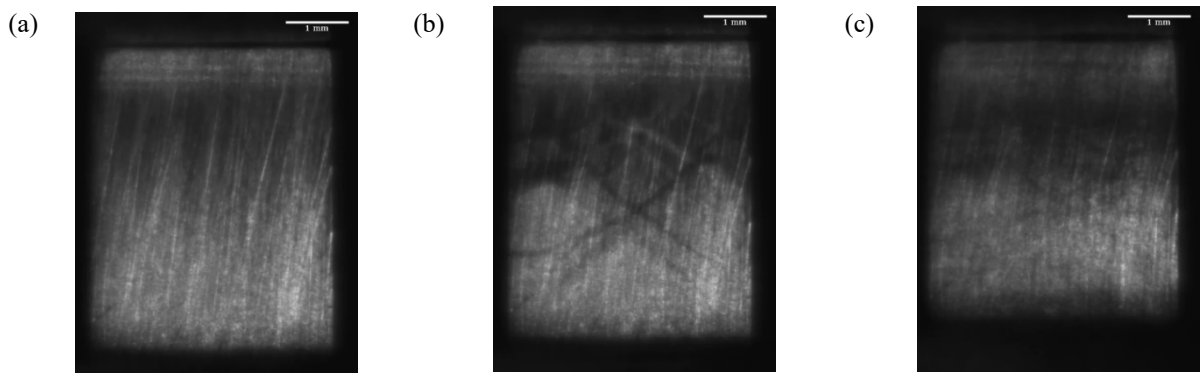

Figure 2. Surface of HSLA 65 specimen in quasi-static compression using a MTS 810 universal testing machine at a strain rate of 10^{-3} s^{-1}: Image a) surface of the specimen before deformation; b) surface of the specimen with localizations fully developed at ~4.6% strain; and c) surface of the specimen after formation of bands as surface texturing develops at ~11% strain demonstrating that the shear bands are consumed and are barely visible.

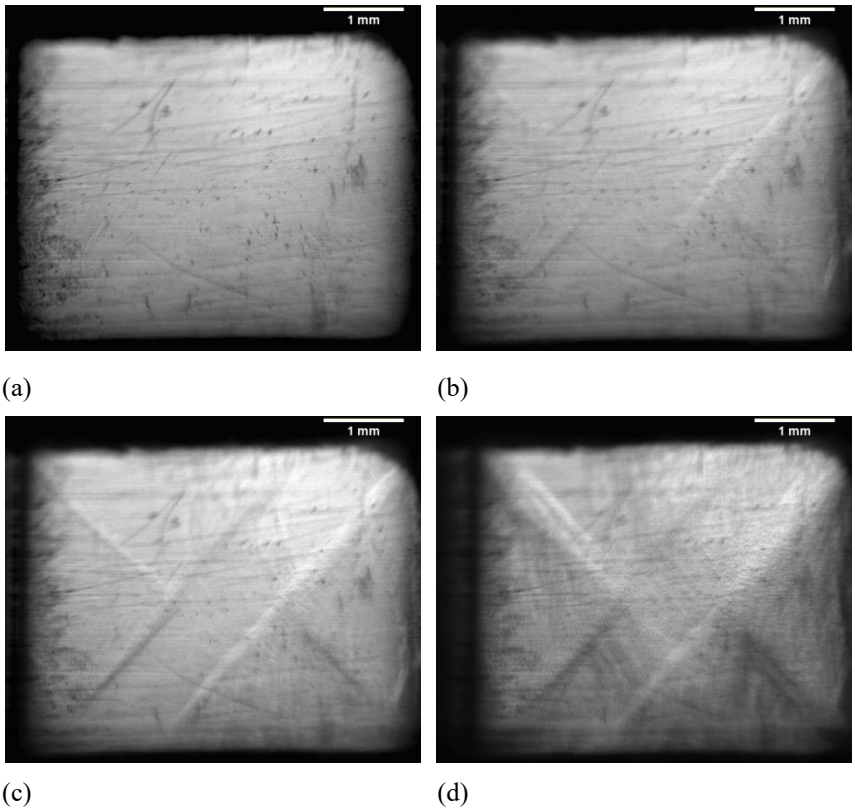

Figure 3. In-situ images of HSLA 65 using Kirana ultra-high-speed camera filming at 1 million frames per second in a Split Hopkinson pressure bar testing apparatus: a) surface of specimen prior to deformation; b) surface of specimen with bands beginning to form at ~1% strain; c) surface of specimen with bands formed before coalesce dominates at ~2% strain; d) surface of specimen with visible localizations and surface texturing at ~3.9% strain.

Using ImageJ [24,25], the initiation and growth of shear bands were tracked over multiple frames for both quasi-static and dynamic loading. The velocity of the localizations on the surface is plotted against the compressive strain for both strain rates in Figure 4, with the range of the strain they occur over denoted in Figure 1 as red vertical lines. The measurements were taken until the originally pristine surface was filled with the larger bands. At this point, coalescence is predominant and the resulting shear

bands are not included in the analysis. In the quasi-static case, the shear bands begin to form on the surface at approximately 2.5% strain and accelerate from a velocity of 27 ± 5 mm/s to 38 ± 8 mm/s at a strain of 2.51%. Following this, the band growth slows to 19 ± 4 mm/s and stays approximately constant over the next 0.01% strain, at which it slows to 11 ± 2 mm/s before meeting other localizations seen on the surface at a strain of 2.71%. Again, these measurements are shown as black dots in Figure 4.

For the dynamic case (blue dots in Figure 4), the shear bands are tracked from ~1.24% to ~2.58% strain, and this occurs approximately over 4 μs during the experiment. The shear band velocity measurements for the dynamic cases are shown as black points in Figure 4. In this plot, the error bars correspond to the bias uncertainty in the calculation, including the camera resolution, variation in time for each frame, and in the dynamic case the random error in repeated measurements of the length of the band between experiments. These errors provide the variation in calculated shear band growth velocities given the short time scales over which they are calculated. The first measurement of velocity is 951 ± 96 m/s at approximately 1.24% strain, where the growth of the band accelerates for the next two frames to 1911 ± 192 m/s at 1.46% strain and 2122 ± 213 m/s at 1.92% strain. At the third frame, the band growth begins to decelerate, when it reaches approximately 2% strain and finally ends at 1464 ± 147 m/s. After this time, the bands may arrest after fully forming on the surface and the energy may be transformed into heat, further deformation and grain alterations [26]. Relating the strain measurement from the images to the stress-strain curves, the pace of growth begins and increases at the point of yield and slows near the trough of the softening (see Figure 1). Generally, the velocity first accelerates as new bands begin forming on the surface and decelerates until coalescence begins.

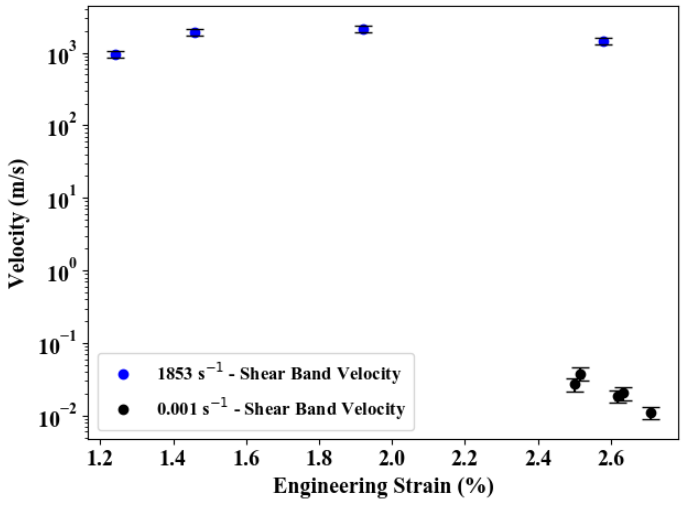

Figure 4. Velocity of shear bands on the surface of the specimens in quasi-static and dynamic compression where the first and last points for each respective case correspond to the lines on the stress-strain curve provided in Figure 1.

4. Discussion

In this paper, we explored the strain rate-dependent compression response of HSLA 65 naval steel, focusing on shear bands and failure. Consideration of the stress-strain response found that the yield strength is 541 ± 8 MPa for quasi-static and 1081 ± 48 MPa for dynamic rates, the K is 2029 ± 172 MPa for quasi-static and 3098 ± 52 MPa for dynamic rates, and the hardening exponent n is 0.376 ± 0.028 for quasi-static and 0.396 ± 0.006 for dynamic rates. These measurements are consistent with those reported in the literature for HSLA 65 [27], and they demonstrate that the HSLA 65 steel is comparable to common naval steels such as HY-80 [28] and DH36 [29].

To explore material responses further, mechanical testing was coupled to high-speed imaging of the specimen surface to investigate shear banding and failure in HSLA 65. To do this, the initiation and growth of the bands were tracked using ImageJ, and the resulting growth rates were plotted against compressive strain (Figure 4). In the quasi-static case, the shear bands begin to form on the surface of the specimen at approximately 2.5% strain and accelerate to a peak of 38 ± 8 mm/s at a strain of 2.51%. Following this, the band growth slows to 19 ± 4 mm/s and stays approximately constant over the next 0.01% strain, at which it

slows 11 ± 2 mm/s before coalescing with other localizations observed on the surface at a strain of 2.71%. For dynamic strain rates of 1853 ± 31 s^{-1}, the bands begin to grow at approximately 1.2% strain, and they accelerate up to 2122 ± 213 m/s at 1.9% strain. Following this, the bands decelerate and then are consumed by deformation on the surface of the specimen. Relating the strain measurement from the images to the stress-strain curves, the pace of growth begins and increases at the point of yield and slows near the trough of the softening (see Figure 1 and Figure 4). Altogether, results from this paper will be important in the development of models, both for phenomenological [30] and for those models that capturing shear banding in steels [31,32].

The peak velocity of 2122 ± 213 m/s is 68% of the shear wave speed, which is acceptable to values of 40 to 67% that are commonly reported in the literature [9,10,33]. While numerical simulations show generally good agreement with experimental studies, shear band velocities in simulations have been shown to be higher using methods which do not require mesh generation [33]. In the study by Li et al. [33], a better curvature match is found in regards to Zhou et al. [9] experimental work, although the peak velocity was found to be 2005 m/s with an impact velocity of 35 m/s. Coupled with the current work, it may be plausible that the shear bands can meet or exceed previously found velocity values in the experimental literature. Namely, the shear band velocities found is this study are higher than those velocities found in studies relating to Maraging c300 steel by Zhou et al. [9], who found at a peak velocity of 1200 m/s with the same acceleration pattern that was found in this study even given the smaller time window our measurements exist within. In a separate study by Guduru et al. [10] also using Maraging c300 steel found the peak velocity to be 1100 m/s, although they found that the generated shear band momentarily slowed down and then proceeded to accelerate again. This behavior is not seen in our current work or in the work of Zhou et al. [9]. Our study also did not observe fracturing from the shear band, which was noted in the works by Zhou et al. [9] and Guduru et al. [10].

5. Concluding Remarks

In this paper, we investigate the dynamic failure and shear banding in HSLA 65 steel. To accomplish this, we performed strain-rate dependent compression measurements on the material and coupled high-speed and ultra-high-speed cameras to monitor the initiation and growth of shear bands during testing. These observations were linked to measurements of the stress-strain response of the materials. Results indicate that the yield strength increases from 541 ± 8 MPa for quasi-static (10^{-3} s^{-1}) to 1081 ± 48 MPa for dynamic rates (1853 ± 31 s^{-1}), and the hardening exponent increases from 0.376 ± 0.028 for quasi-static to 0.396 ± 0.006 for dynamic rates. The yield in the material was observed to be associated with the onset and evolution of shear banding in HSLA 65. For the quasi-static case, shear banding and yielding was observed to occur at 2.5% and 0.93 ± 0.12 % strain, respectively and these can reach speeds of upwards of 38 mm/s. For the dynamic experiments, the shear banding begins at approximately 1.18 ± 0.06% strain and these can grow upwards of 2122 ± 213 m/s. Altogether, this study provides new insights into shear banding and dynamic failure of steel materials, which is useful in manufacturing and modelling of these materials.

Acknowledgements

This work is supported by the Canadian Natural Sciences and Engineering Research Council, the Canadian Foundation for Innovation, and Defence Research and Development Canada. Calvin Lo and Haoyang Li are thanked for their aid while running the experiments.

References

[1] Mendoza, I., Villalobos, D., and Alexandrov, B. T., 2015, "Crack Propagation of Ti Alloy via Adiabatic Shear Bands," Materials Science and Engineering: A, **645**, pp. 306–310.

[2] Latourte, F., Feinberg, Z., Mori, L. F., Olson, G. B., and Espinosa, H. D., 2010, "Shear and Tensile Plastic Behavior of Austenitic Steel TRIP-120 Compared with Martensitic Steel HSLA-100," International Journal of Fracture, **162**(1–2), pp. 187–204.

[3] Nakkalil, R., Hornaday, J. R., and Bassim, M. N., 1991, "Characterization of the Compression Properties of Rail Steels at High Temperatures and Strain Rates," Materials Science and Engineering: A, **141**(2), pp. 247–260.

[4] Odeshi, A. G., Owolabi, G. M., and Nabil Bassim, M., 2007, "Effects of particulate reinforcement and strain-rates on deformation and fracture behavior of Aluminum 6061-T6 under high velocity impact," Materialwissenschaft und Werkstofftechnik, **38**(2), pp. 66–69.

[5] Odoh, D., Owolabi, G., Odeshi, A., and Whitworth, H., 2013, "Shear Band Formation in AISI 4340 Steel under Dynamic Impact Loads: Modeling and Experiment," Acta Metallurgica Sinica (English Letters), **26**(4), pp. 378–384.

[6] Nakkalil, R., 1991, "Formation of Adiabatic Shear Bands in Eutectoid Steels in High Strain Rate Compression," Acta Metallurgica et Materialia, **39**(11), pp. 2553–2563.

[7] Swallowe, G. M., 2012, "Adiabatic Shear Bands in Polymers," *Adiabatic Shear Localization*, Elsevier, pp. 363–398.
[8] Fakhimi A., Riedel J. J., and Labuz J. F., 2006, "Shear Banding in Sandstone: Physical and Numerical Studies," International Journal of Geomechanics, **6**(3), pp. 185–194.
[9] Zhou, M., Rosakis, A. J., and Ravichandran, G., 1996, "Dynamically Propagating Shear Bands in Impact-Loaded Prenotched Plates—I. Experimental Investigations of Temperature Signatures and Propagation Speed," Journal of the Mechanics and Physics of Solids, **44**(6), pp. 981–1006.
[10] Guduru, P. R., Rosakis, A. J., and Ravichandran, G., 2001, "Dynamic Shear Bands: An Investigation Using High Speed Optical and Infrared Diagnostics," Mechanics of Materials, **33**(7), pp. 371–402.
[11] Wright, T. W., and Batra, R. C., 1985, "The Initiation and Growth of Adiabatic Shear Bands," International Journal of Plasticity, **1**(3), pp. 205–212.
[12] Arriaga, M., McAuliffe, C., and Waisman, H., 2016, "Instability Analysis of Shear Bands Using the Instantaneous Growth-Rate Method," International Journal of Impact Engineering, **87**, pp. 156–168.
[13] Owolabi, G., Odoh, D., Odeshi, A., and Whitworth, H., 2013, "Occurrence of Dynamic Shear Bands in AISI 4340 Steel under Impact Loads," World Journal of Mechanics, **03**(02), pp. 139–145.
[14] Hines, J. A., and Vecchio, K. S., 1997, "Recrystallization Kinetics within Adiabatic Shear Bands," Acta Materialia, **45**(2), pp. 635–649.
[15] Meyers, M. A., Xu, Y. B., Xue, Q., Pérez-Prado, M. T., and McNelley, T. R., 2003, "Microstructural Evolution in Adiabatic Shear Localization in Stainless Steel," Acta Materialia, **51**(5), pp. 1307–1325.
[16] Syn, C. K., Lesuer, D. R., and Sherby, O. D., 2005, "Microstructure in Adiabatic Shear Bands in a Pearlitic Ultrahigh Carbon Steel," Materials science and technology, **21**(3), pp. 317–324.
[17] Xu, Y. B., Bai, Y. L., Xue, Q., and Shen, L. T., 1996, "Formation, Microstructure and Development of the Localized Shear Deformation in Low-Carbon Steels," Acta Materialia, **44**(5), pp. 1917–1926.
[18] Dolinski, M., Merzer, M., and Rittel, D., 2015, "Analytical Formulation of a Criterion for Adiabatic Shear Failure," International Journal of Impact Engineering, **85**(Supplement C), pp. 20–26.
[19] A01 Committee, *Specification for High-Strength Low-Alloy Structural Steel Plate with Low Carbon and Restricted Sulfur for Improved Weldability, Formability, and Toughness*, ASTM International.
[20] Štamborská, M., Kvíčala, M., and Losertová, M., 2014, "Identification of the Mechanical Properties of High-Strength Steel Using Digital Image Correlation," Advanced Materials Research, **980**, pp. 122–126.
[21] Chen, W. W., and Song, B., 2011, *Split Hopkinson (Kolsky) Bar: Design, Testing and Applications*, Springer, New York, NY.
[22] Panowicz, R., Janiszewski, J., and Kochanowski, K., 2018, "Influence of Pulse Shaper Geometry on Wave Pulses in SHPB Experiments," Journal of Theoretical and Applied Mechanics, **56**(4), pp. 1217–1221.
[23] ASM International, Kuhn, H., and ASM International, eds., 2000, *Mechanical Testing and Evaluation*, ASM International, Materials Park, Ohio.
[24] Schneider, C. A., Rasband, W. S., and Eliceiri, K. W., 2012, "NIH Image to ImageJ: 25 Years of Image Analysis," Nature Methods, **9**(7), pp. 671–675.
[25] Schindelin, J., Arganda-Carreras, I., Frise, E., Kaynig, V., Longair, M., Pietzsch, T., Preibisch, S., Rueden, C., Saalfeld, S., Schmid, B., Tinevez, J.-Y., White, D. J., Hartenstein, V., Eliceiri, K., Tomancak, P., and Cardona, A., 2012, "Fiji: An Open-Source Platform for Biological-Image Analysis," Nature Methods, **9**(7), pp. 676–682.
[26] Longère, P., 2017, "Respective/Combined Roles of Thermal Softening and Dynamic Recrystallization in Adiabatic Shear Banding Initiation," Mechanics of Materials.
[27] Nemat-Nasser, S., and Guo, W.-G., 2005, "Thermomechanical Response of HSLA-65 Steel Plates: Experiments and Modeling," Mechanics of Materials, **37**(2–3), pp. 379–405.
[28] Conn, A. F., Rudy, S. L., and Howard, S. C., 1974, *THE STRAIN RATE DEPENDENCE OF THREE HIGH STRENGTH NAVAL ALLOYS*, T. R. 7111-1, Office of Naval Research Department of the Navy.
[29] Nemat-Nasser, S., and Guo, W.-G., 2003, "Thermomechanical Response of DH-36 Structural Steel over a Wide Range of Strain Rates and Temperatures," Mechanics of Materials, **35**(11), pp. 1023–1047.
[30] Daridon, L., Oussouaddi, O., and Ahzi, S., 2004, "Influence of the Material Constitutive Models on the Adiabatic Shear Band Spacing: MTS, Power Law and Johnson–Cook Models," International Journal of Solids and Structures, **41**(11–12), pp. 3109–3124.
[31] Batra, R. C., 2012, "Analysis of Adiabatic Shear Bands by Numerical Methods," *Adiabatic Shear Localization*, Elsevier, pp. 173–214.
[32] Medyanik, S. N., Liu, W. K., and Li, S., 2007, "On Criteria for Dynamic Adiabatic Shear Band Propagation," Journal of the Mechanics and Physics of Solids, **55**(7), pp. 1439–1461.
[33] Li, S., Liu, W. K., Rosakis, A. J., Belytschko, T., and Hao, W., 2002, "Mesh-Free Galerkin Simulations of Dynamic Shear Band Propagation and Failure Mode Transition," International Journal of Solids and Structures, **39**(5), pp. 1213–1240.
[34] Hunter, J. D., 2007, "Matplotlib: A 2D Graphics Environment," Computing In Science & Engineering, **9**(3), pp. 90–95.